Dynamics of beating cardiac tissue under slow periodic drives

Po-Yu Chou,[1] Wei-Yin Chiang,[1] C. K. Chan,[2,*] and Pik-Yin Lai[1,†]
[1]*Department of Physics, and Center for Complex Systems, National Central University, Chungli District, TaoYuan City 320, Taiwan, Republic of China*
[2]*Institute of Physics, Academia Sinica, Nankang, Taipei 115, Taiwan, Republic of China*

(Received 3 March 2019; published 3 January 2020)

Effects of mechanical coupling on cardiac dynamics are studied by monitoring the beating dynamics of a cardiac tissue which is being pulled periodically at a pace slower than its intrinsic beating rate. The tissue is taken from the heart of a bullfrog that includes pacemaker cells. The cardiac tissue beats spontaneously with an almost constant interbeat interval (IBI) when there is no external forcing. On the other hand, the IBI is observed to vary significantly under an external periodic drive. Interestingly, when the period of the external drive is about two times the intrinsic IBI of the tissue without pulling, the IBI as a function of time exhibits a wave packet structure. Our experimental results can be understood theoretically by a phase-coupled model under external driving. In particular, the theoretical prediction of the wave-packet period as a function of the normalized driving period agrees excellently with the observations. Furthermore, the cardiac mechanical coupling constant can be extracted from the experimental data from our model and is found to be insensitive to the external driving period. Implications of our results on cardiac physiology are also discussed.

DOI: 10.1103/PhysRevE.101.012201

I. INTRODUCTION

It is well known that our hearts do not beat with a constant rate and its variability known as heart rate variability (HRV) has long been investigated for both its clinical significance [1] and fundamental mechanism [2]. HRV is measured by the fluctuations in the interbeat interval (IBI) in time, and is an important physiological indicator. A low HRV often is a predictor of mortality after myocardial infarction and often correlated to other cardiac related diseases such as congestive heart failure, postcardiac transplant, susceptibility to sudden infant death syndrome and poor survival in premature babies. It is generally believed that HRV reflects the physiological state of our nervous control system and therefore can be used as an index of our health. With this picture, a high HRV signifies a high complexity or flexibility in our nervous control system and therefore indicates a state of well-being of our health. For example, a patient in an intensive care unit has a very small HRV even if the heart can beat on its own, whereas meditation [3] can supposedly enhance one's HRV and therefore health. In recent years, continuous monitoring of HRV by wearable electronic devices is a common health biomarker. Hence a deeper understanding of the IBI cardiac dynamics would be important for both the fundamental physiological HRV dynamics and for medical purposes. HRV is closely related to a phenomenon known as RSA (respiration sinus arrhythmia) [4] in which our heart rate increases during inhalation and vice versa. The mechanism of RSA is still not clear but it is generally believed that it is through the activation and deactivation of the sympathetic and parasympathetic nerve system [5] through our respiration that modulates the heart rate. However, there is another effect of respiration on cardiac beating, namely the periodic mechanical stress created in our chest. For example, the respiration of a pregnant woman might provide the common drive for modulating her and the fetus's heart rates through mechanical stresses [6].

On the tissue level, the pacemaking of a heart beat originates from the sinus atrial node (SAN) [7]. Interestingly, the SAN is not a well defined organ, but is a cluster of cardiac myocytes (CMs) and fibroblasts (FBs). A CM is an electrically excitable cell which is responsible for mechanical contraction of the heart. A FB is not electrically excitable but is known for its mechanical sensitivity [8]. However, it is still not clear what is the function of the mechanical sensitivity of the FB although it is known that coupling among CMs and FBs can regulate the beating frequencies of the cardiac tissue [9]. In a normal functioning heart, the beating is generated from the SAN controlled by parasympathetic and sympathetic nerves. However, the SAN is an oscillatory medium and it can still generate its own beat as in the case of an isolated heart preparation where all nerves connected to the heart are severed. Although HRV dynamics is regulated by various other physiological systems such as the sympathetic and parasympathetic nerves, blood pressure, etc., HRV still persists in isolated hearts [10] which presumably is due to intrinsic intracardiac factors that affect the cardiac rhythm. One possible origin of the HRV in an isolated heart is that there is a feedback from the FB to the pacemaking dynamics of the SAN modulated by the mechanical stress experienced by the FB in the SAN.

From another perspective, it was known that cardiac massage could revive sudden circulatory arrests since the early 20th century [11]. Such a first-aid procedure not only can help blood pumping and prevent the brain from hypoxia, it

*ckchan@gate.sinica.edutw
†pylai@phy.ncu.edu.tw

also enhances heart rate regulations [12] that involve possible mechanoelectric feedback processes, in which the mechanical stimulus is transduced into an electrical signal [13,14] and in turn revives the cardiac system to beat normally. The contractile force of the intact natural heart tissue depends on the species; it is around few tens mN/mm^2 [15,16] for mammals such as human, rabbit, and rats, and is around a few mN/mm^2 for frogs [17]. For those engineered cardiac tissues, such as those employing iPSC technology, the force is an order of magnitude smaller [18]. Thus it is of interest to investigate the effects of external stretching forces with comparable magnitudes on the beating dynamics. Studies have been focused on the stretch response in different levels; *in vivo* [19], tissue level [20], and single cell level [21,22], the effects of stretching on the diastolic depolarization rate, beating rate, and the value of maximal systolic potential [23,24] were investigated. On the cellular level, several processes are involved in response to the stretching of cardiac cells, such as integrin binding on cell surface followed by signal trigger and cation flow induced by stretched-activated channel. Experiments on cardiac cells under periodic electrical stimulus have been performed [25] focusing on the phase-locking between external stimulus and cardiac cell, and period-doubling of beating rates were observed and analyzed theoretically by using a phase variable in a circle map.

In this work, we focus on the dynamical response of cardiac tissue under external cyclic pulling, and aim to understand the dynamics of beating, interbeat interval (IBI), under different driving periods by employing a phase-coupled model. We find that the dynamics of IBI under suitable periodic pulling is in the form of a "wave packet," with the period of the wave packet ($T_{\rm wp}$) being a function of the external driving period ($T_{\rm drive}$). A remarkable feature is that $T_{\rm wp}$ seems to be maximal when $T_{\rm drive} \sim 2T_0$ where T_0 is the intrinsic beating period of the cardiac tissue. A phase model, with the key parameter being the coupling constant (K) between the phases of beating and external pulling, is then developed which can quantitatively describe our experimental findings well. In addition, the amplitude of the wave packet is found to be related to K, thus allowing the extraction of K from experimental IBI time-series data.

II. EXPERIMENTAL METHOD

The schematic of the experiment is shown in Fig. 1(a). Samples of beating sinus venosus (typical size $\approx$5 mm $\times$ 10 mm) are dissected from bullfrogs. The sample is fixed at one end on a PDMS substrate in a Petri dish by two electrodes (200 μm in diameter and about 1 mm apart) made from insect pins. The other end of the sample is tied to a string which is connected to servomotor. During the experiment, the sample is kept at room temperature and perfused continuously with the Ringer solution (6 g NaCl, 0.2 g Na_2SO_4, 0.2 g KCl, and 0.2 g $CaCl_2$ in 1000 ml of water). The sample can be pulled by the servomotor controlled by a computer while the beatings of the sample are monitored by measuring the local-field potentials obtained from the electrodes. The pulling force is measured by the extension of the spring monitored by a charge-coupled device camera. The stretching force we employed in the experiments is comparable to the contractile

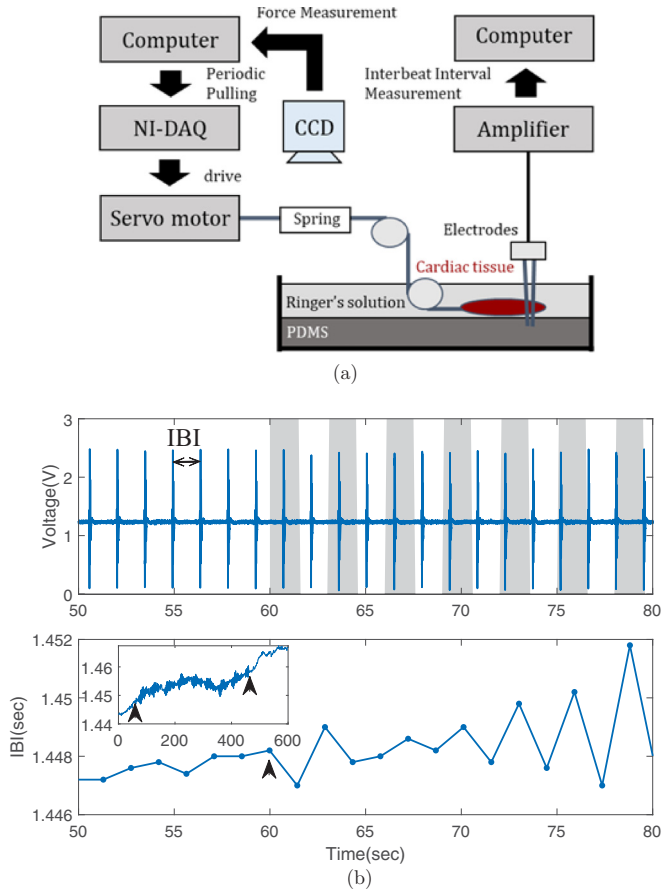

FIG. 1. (a) Schematic experimental setup. (b) Top: Time course of measured local field of potential acquired by the electrodes (blue curve showing 21 beats) from which the interbeating-interval (IBI) is determined. Shaded regions show the periods during which the stretching force is acting on the tissue. Bottom: Time course of the 20 IBIs determined from (a). The insets show the time course of a whole experiment. Periodic stretching force is applied from 60 to 460 s as indicated by arrows. Note that there is a systematic slight increase in IBI due to aging of the sample.

force of the cardiac tissue in order to achieve a non-negligible effect. The typical magnitudes of the stretching force on the cardiac tissue used in the experiment are around few tens to hundreds mN. With the setup described above, the sample can beat for at least 24 h with a systematic increase in IBI because of aging of the sample *in vitro*. Figure 1(b) shows a typical time course of the electrical signals obtained from the electrodes for a pulling experiment. These signals are first amplified (model 1700, A-M Systems, USA) with a low-pass filter (500 Hz) and then recorded by a digital data acquisition system NI-6221 (National Instruments, USA) which was controlled by PowerGraph Professional software (version 3.3.7, Russia) with a 4-kHz sampling rate. The peak locations of the recorded local-field potentials can be determined with a precision of 0.25 ms and therefore the interbeat intervals (IBIs) can be determined with a precision of 0.5 ms. The determined IBI is shown in the bottom panel in Fig. 1(b). Before the start of a pulling experiment, the intrinsic IBI (without pulling) of the sample is monitored for at least 15 min to make sure the sample is adapted to the *in vitro* environment with

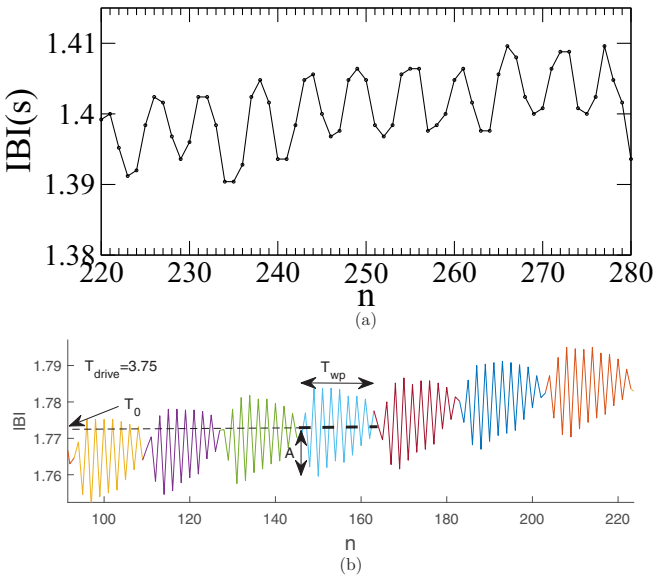

FIG. 2. Time course of IBI for cardiac tissue under external driving of period $T_{\rm drive}$. (a) Very slow driving period with $T_{\rm drive} = 8$ s. The IBIs basically follow the external driving. (b) For $T_{\rm drive}$ of the order of twice the intrinsic beating period, the wave-packet pattern appears. The instantaneous intrinsic beating period (T_0) of the cardiac tissue is obtained by averaging the interbeat intervals over one wave packet.

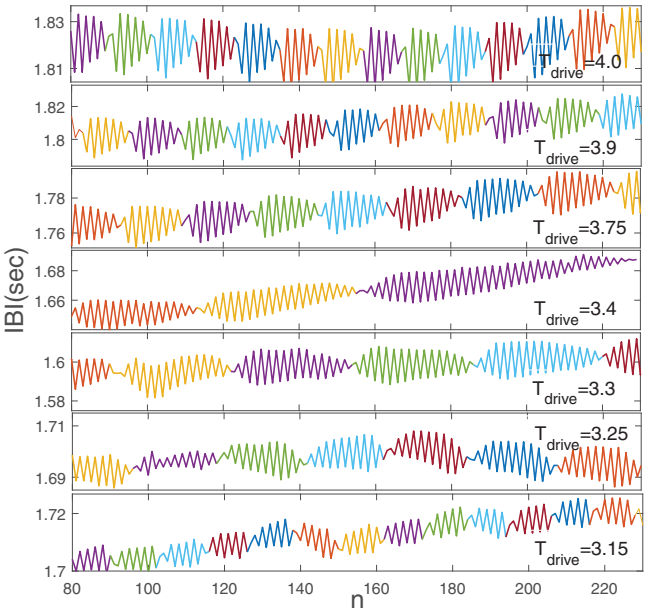

FIG. 3. Time course of the interbeat intervals obtained from local-field potential of the same cardiac tissue under different external stretching periods. The wave-packet period varies with the stretching period nonmonotonically.

an almost constant intrinsic IBI. In the experiments reported below, the duration for each pulling experiment trial is 600 s; periodic stretching is applied between the 60th second and the 460th second.

III. EXPERIMENTAL RESULTS

It is convenient to describe the time course of the beating dynamics in terms of the beat number n. The nth beat is defined as the nth peak voltage measured which occurs at time T_n. The nth IBI is then defined as the difference between two consecutive beating times $T_{n+1} - T_n$. By applying a periodic stretching, the beating cardiac tissue responds to the external driving by changing its IBIs. For very slow driving periods, the IBIs show modulations that follow the external driving as shown in Fig. 2(a). Notice again that there is a systematic drift in the IBI oscillations, presumably due to the slow aging of the cardiac tissue. Remarkably, for driving with $T_{\rm drive}$ of the order twice that of the intrinsic beating period, the IBIs display a wave-packet pattern as shown in Fig. 2(b). Each wave packet basically consists of alternating high and low values of IBIs, i.e., IBI alternans, with the amplitude being modulated by a slow wave-packet period ($T_{\rm wp}$). When the external stretching period is varied, different periods of wave packet are observed as displayed in Fig. 3. Interestingly, the period of wave packet changes nonmonotonically with the driving period, and $T_{\rm wp}$ is largest when the stretching period is close to two times the intrinsic beating period.

To quantify the wave-packet pattern, the period of wave packet is measured for different external driving periods. Since the mean IBI for each wave packet is not stationary, a temporal average IBI is measured within a wave packet (denoted by T_0) and regarded as the (instantaneous) intrinsic beating period of the wave packet. The amplitude of the wave packet, denoted by A, is also measured for each wave packet from the maximal magnitude of IBI deviated from the mean IBI within the wave packet [see Fig. 2(b)]. The periods of the wave packets under different driving periods are measured and the results are displayed in Fig. 4. For a given external driving frequency, one can obtain a set of data with a range of values of $T_{\rm drive}/T_0$ depending on how much the intrinsic

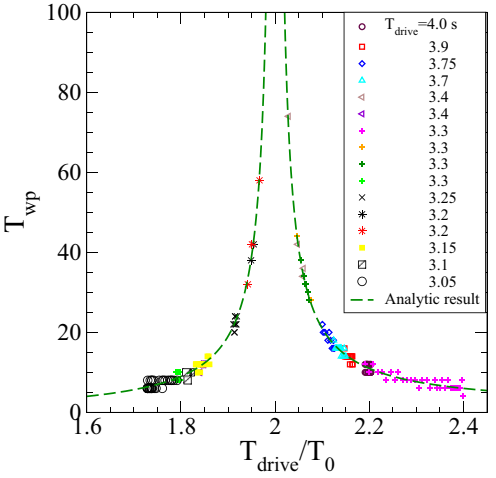

FIG. 4. The wave packet periods($T_{\rm wp}$) obtained from experimental data of the IBI dynamics, plotted against the ratio of the driving period to the intrinsic beating period. The intrinsic heart beating rate is nonstationary and drifts with time, thus the intrinsic period (T_0) is temporally defined within one period of wave packet. All the data for $T_{\rm wp}$ collapse into a master curve that depends on the ratio of $T_{\rm drive}/T_0$ and diverges at $T_{\rm drive}/T_0 = 2$. The dashed curve is the analytic formula from (8) showing excellent agreement.

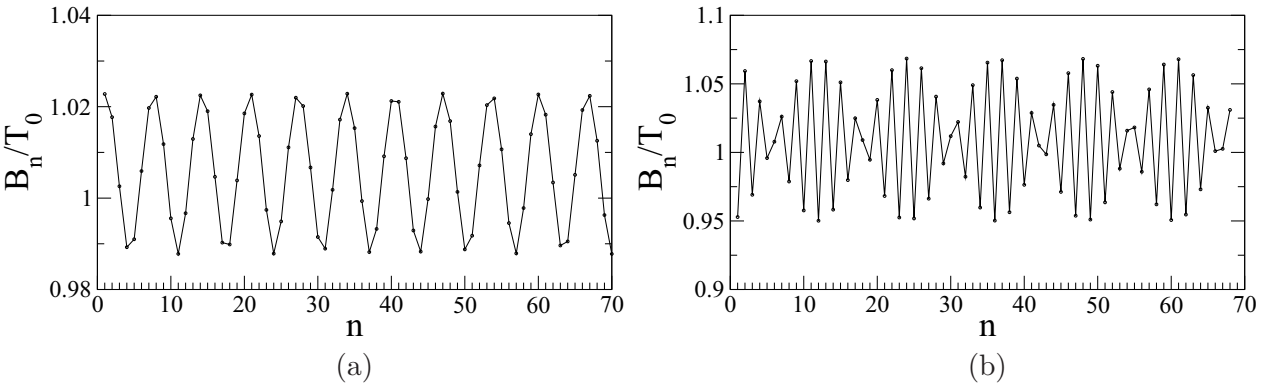

FIG. 5. Interbeat interval (B_n), in unit of the intrinsic beating period $T_0 = \frac{2\pi}{\omega}$, as a function of beat number obtained by $T_{n+1} - T_n$, where T_n are the successive roots found in Eq. (4). Coupling constant $\frac{K}{\omega} = 0.1$. (a) $\omega/\Omega = 6.6$ and (b) $\omega/\Omega = 2.2$.

beating period drifts. Figure 4 shows the experimental results of the measured $T_{\rm wp}$ (in units of beats) plotted as a function of $T_{\rm drive}/T_0$ for various driving periods. Remarkably all the data collapse into a master curve and the wave-packet period appears to diverge at $T_{\rm drive}/T_0 \approx 2.$ and appears to be independent of the mechanical coupling between the tissue and the external driving, since the data are from different animals. The divergence of $T_{\rm wp}$ near $T_{\rm drive}/T_0 \simeq 2$ simply indicates a pure (unmodulated) IBI alternans state of alternating high and low IBIs.

IV. PHASE MODEL FOR CARDIAC TISSUE UNDER PERIODIC FORCING

In order to understand theoretically the experimental results, we employ a phase model to describe the response of the beating dynamics of the cardiac tissue under an external periodical mechanical stretching. Denote the phase and the intrinsic frequency (i.e., under no external forcing) of the beating tissue by $\phi(t)$ and ω respectively; the tissue is phase-coupled to the external driving oscillator of frequency Ω, and the dynamics is governed by the following equations:

$$\dot{\phi} = \omega + K\sin(\Phi - \phi), \quad \dot{\Phi} = \Omega, \tag{1}$$

where $K > 0$ is the coupling constant and Φ is the phase of the external periodic device that provides the stretching. The dynamics of this system can be better understood in terms of the phase difference, $\psi(t) \equiv \phi(t) - \Omega t$, and (1) can be reduced to

$$\dot{\psi}(t) = \omega - \Omega - K\sin\psi. \tag{2}$$

It is convenient to define the dimensionless coupling $\tilde{K} \equiv \frac{K}{\omega-\Omega}$ for further theoretical analysis. It should be noted that (1) is the same as the firefly entrainment model [26] for the synchronization of an oscillator under external periodic drive. For $|\tilde{K}| > 1$, entrainment can be achieved with the existence of stable fixed point and the oscillator is phase-locked with the external drive with $\psi = \sin^{-1}(\tilde{K}^{-1})$. For Ω near ω, the cardiac tissue lies in the entrainment regime and will simply follow a compromised frequency that lies between ω and Ω. However, as will be shown in next section, the coupling is small ($K \ll \omega$) for this cardiac system, the entrainment regime is very narrow. Here we focus on the much less studied oscillatory phase drift behavior for the asynchronized dynamics, and in particular on the situation of slow driving with $\Omega < \omega$ and the weak-coupling regime of $0 < \tilde{K} < 1$. $\psi(t)$ in (2) can be integrated analytically to give

$$\tan\frac{\psi(t)}{2} = \tilde{K} + \sqrt{1-\tilde{K}^2}\,\frac{\tan\left[\frac{\sqrt{1-\tilde{K}^2}}{2}(\omega-\Omega)t\right] - \beta}{1 + \beta\tan\left[\frac{\sqrt{1-\tilde{K}^2}}{2}(\omega-\Omega)t\right]}, \tag{3}$$

where β is a constant determined by the initial condition. For $\psi(0) = 0$, $\beta = \frac{\tilde{K}}{\sqrt{1-\tilde{K}^2}}$. Define T_n as the time for the nth beat to occur, and the origin of ϕ can be chosen such that $\phi(T_n) = 2n\pi$, then at $t = T_n$, $\psi(T_n) \equiv \psi_n = 2n\pi - \Omega T_n$, and (3) can be reduced to (see Appendix A for a detailed derivation)

$$\tan\frac{\Omega T_n}{2} + \tilde{K} + \sqrt{1-\tilde{K}^2}\,\frac{\tan\left[\frac{\sqrt{1-\tilde{K}^2}}{2}(\omega-\Omega)T_n\right] - \beta}{1 + \beta\tan\left[\frac{\sqrt{1-\tilde{K}^2}}{2}(\omega-\Omega)T_n\right]} = 0. \tag{4}$$

T_n can be obtained from the roots of the transcendental equation (4). The nth IBI (denoted by B_n) is then given by $T_{n+1} - T_n$. The roots of the transcendental equation (4) are obtained numerically and the time course of B_n is shown in Fig. 5 for two driving frequencies. For very slow driving frequency ($\omega/\Omega = 6.6$), the IBI variation simply follows the slow driving frequency, agreeing with experimental observations, as shown in Fig. 5(a). On the other hand, B_n displays the characteristic wave-packet structure similar to experimental observation when Ω is of the order of $\omega/2$ [Fig. 5(b)].

In order to gain a deeper connection between the theoretical model and the experimental data, we derive an explicit analytic formula for B_n using systematic expansion in powers of $\tilde{K}$ (details of the derivation are shown in Appendix B). To first order in $\tilde{K}$, we obtain the formula

$$B_n \approx \frac{2\pi}{\omega} + \frac{2\tilde{K}}{\omega}\sin\left(\frac{\Omega\pi}{\omega}\right)\sin\left[\frac{\Omega}{\omega}(2n+1)\pi\right] + \mathcal{O}(\tilde{K}^2). \tag{5}$$

One can see clearly that even under the first-order approximation of K, B_n fluctuates about $2\pi/\omega$ with an

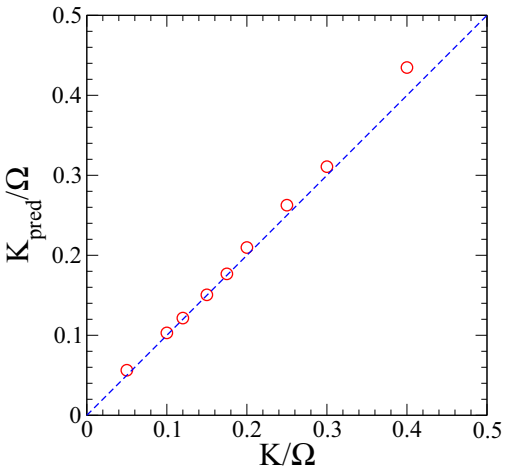

FIG. 6. Validation of the extraction of the coupling from the wave-packet amplitude in the time course of IBI. The predicted coupling (in unit of Ω, symbols) obtained by measuring the amplitude of the wave packet in numerical solution [using (1)] for given K (also in unit of Ω). The dashed line indicates the $y = x$ line is a guide to the eyes. Coupling constant K can be accurately extracted for low values of K/Ω up to $K/\Omega \sim 0.4$.

amplitude of $\frac{2\tilde{K}}{\omega}\sin\frac{\Omega\pi}{\omega}$ modulated by the $\sin[\frac{\Omega}{\omega}(2n+1)\pi]$ term. Therefore, by measuring the amplitude (denoted by A) of the wave packets of the IBIs [see Fig. 2(b)], the coupling constant K can be inferred using

$$K = \frac{A}{2}\frac{\omega(\omega-\Omega)}{\sin\left(\frac{\Omega}{\omega}\pi\right)}. \tag{6}$$

To find out the range of validity of the above extraction of K from the time course of B_n via Eq. (6), we first generate the time-series data of B_n for some fixed value of K from the numerical solution of (1) to produce the wave packets, then the amplitude of the wave packets is measured to give an extracted value of K ($K_{\text{predicted}}$) from (6). The extracted $K_{\text{predicted}}$ is then compared with the known K and the results are shown in Fig. 6; the agreement is very good for low values of K up to $K/\Omega \sim 0.4$. Thus for small mechanical couplings, the first-order approximation in (5) would allow accurate extraction of the coupling constant between the external driving and the cardiac tissue from experimental data. Figure 7(a) displays the experimentally extracted coupling constants K via Eq. (6) by measuring the amplitudes of the wave packets for cardiac tissues from five different samples as a function of the external driving period. The inferred K (in units of s^{-1}) values show some scattering but in general the couplings are small and insensitive to the external driving period, justifying the use of expansion to first order in $\tilde{K}$ in (5). We further perform experiments on the same cardiac tissue and with periodic stretching of two different force magnitudes. The extracted K is shown as a function of T_{drive} in Fig. 7(b), showing the coupling constant is also insensitive to the magnitude of force, thus justifying the use of a phase model as our theoretical basis.

In order to show that our model is capable of describing the detailed dynamical behavior quantitatively in the cardiac tissue of sinus venosus in a bullfrog, we derive an analytic result to account for the universal feature of the wave-packet periods shown in Fig. 4, and the divergence at $T_{\text{drive}}/T_0 \approx 2$. From (5), the oscillating term can be rewritten to give

$$\sin\left[\frac{\Omega}{\omega}(2n+1)\pi\right] = (-1)^n \cos\left[(2n+1)\pi\left(\frac{\Omega}{\omega}-\frac{1}{2}\right)\right], \tag{7}$$

revealing that the alternating term $(-1)^n$ is being modulated with a "wave-packet" period of (in unit of beat number)

$$T_{\text{wp}} = \frac{\omega}{\Omega}\frac{1}{\left|2-\frac{\omega}{\Omega}\right|}. \tag{8}$$

$T_{\text{wp}} \to \infty$ simply means that the IBIs alternate between a high and a low value, i.e., a pure IBI alternans state. In fact, it can shown that T_{wp} diverges at $\omega = 2\Omega$ even if higher orders in $\tilde{K}$ are included in the calculations.

V. SUMMARY AND DISCUSSION

In this paper, the dynamical response of a beating tissue of sinus venosus from a bullfrog under periodic stretching with different periods is measured experimentally. By

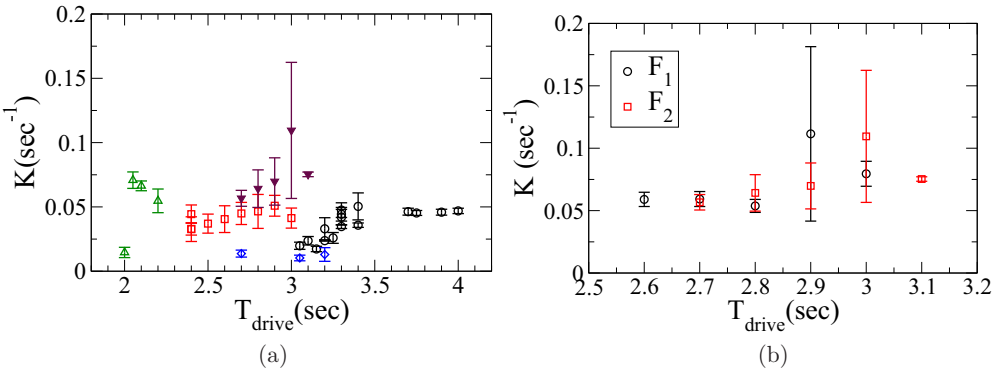

FIG. 7. Extracted coupling strength from Eq. (6). By measuring the amplitudes of the wave packets, coupling strengths between tissue and external driving are extracted from experimental data through Eq. (6). (a) Inferred coupling strengths (in unit of s^{-1}) as a function of driving period, for five different tissue samples. (b) Inferred coupling constant under two different force magnitudes on the same tissue. $F_1 \simeq 0.062N$ and $F_2 \simeq 0.112N$.

applying a periodic stretch on cardiac tissue, IBIs are immediately modified. A wave-packet structure is observed under a suitable driving period. We then develop a theoretical model to understand this interesting phenomenon. By utilizing a phase model to describe the dynamics of the cardiac tissue coupled to the external periodic driving, our model can produce very well the empirical observations. Furthermore, the analytical results from the model enable us to extract the effective coupling between the cardiac tissue and external forcing from experimental measurements of the IBI time courses. It is found that the measured values of the coupling constant are rather robust for cardiac tissues from different samples, and are insensitive to the external driving frequencies and stretching force strengths. The variation of IBIs form a wave-packet pattern when $T_{\rm drive}$ is of the order of twice the intrinsic beating period T_0, and the wave-packet period $T_{\rm wp}$ appears to diverge at $T_{\rm drive}/T_0 = 2$. Such $T_{\rm wp}$ variation is universal in the sense that the data of the wave-packet periods under different $T_{\rm drive}$ all collapse to a universal curve as a function of $T_{\rm drive}/T_0$, and is well described by the analytic formula (8). On the theoretical side, by solving the roots in the transcendental equation derived from the phase model, the beating times are obtained which in turn gives the IBI dynamics. The theoretical IBIs show wave-packet patterns agreeing with experiment observations. In addition, the amplitude and period of the wave packets are derived analytically by systematic expansion in the coupling, which enable the experimental extraction of the coupling K conveniently.

One would like to explore possible mechanisms of how mechanical stretching can immediately modulate the dynamics of a cardiac tissue, which is probed in this study by a periodical stretching. One possible cellular mechanism is that the periodic stretching activates the stretch-activated channels and hence induces cyclic ion currents. This can be interpreted on the cellular level as the periodic stretching on cardiac tissue inducing cyclic electrical stimuli which in turn regulate the beating dynamics of the cardiac tissue. Since a phase model of circle map has been employed successfully to account for cardiac cells under cyclic electrical stimuli [27,28], the use of the phase model coupled to an external driving in (1) is justified to describe the dynamical response of the tissue under periodic forcing.

Our experimental results indicated that the HRV can be modulated by external periodic mechanical forcing that acts on the tissue level, and hence can provide a convenient means to regulate the cardiac dynamics. Furthermore, coupling strength K can be extracted accurately and conveniently from the amplitude of the IBI wave packet with the analytical derived expression (6). The extracted coupling strengths obtained under different stretching periods and for different tissue samples are found to be relatively weak and the values are rather robust for different tissue samples. Since the amplitude of the wave packet is a measure for the HRV, our theoretical result (6) indicates that a better mechanical coupling can result in higher HRV, and hence a better cardiac physiological condition. Thus our result suggests that on the tissue level, a better mechanical coupling with external stimulus reflects a better cardiac health condition, agreeing with our common belief.

In fact, the detailed biochemical process in cardiac pacemaker consists of two clocks: they are the membrane clock (induced by ion channels on the membrane) and the calcium clock [periodic release of calcium by sarcoplasmic reticulum (SR)], respectively. The calcium released by SR affects directly the membrane clock whereas the influx of calcium through the ion channel on the membrane controls the availability of calcium for SR pumping which in turn affects the calcium clock. These two clocks interact and cross talk with each other, and hence a cardiac pacemaker can be viewed as two coupled oscillators [22,29]. In the present study, we have successfully utilized a phase coupled oscillator system to describe a tissue driven by cyclic external stretch. Presumably, in our experiment, we perturb the membrane clock by stretching which deforms the membrane and activates hyperpolarization-activated cyclic nucleotide-gated channel and various L-type and T-type Ca^2+ channels; as a result the RyR opening probability of the calcium clock is regulated. However, more detailed experiments need to be carried out to confirm this picture. Detailed ionic current information by patch-clamp experiments would be ideal to reveal the intracellular transport and the coupling between the two clocks, however it in practice is highly challenging to perform precise patch-clamp measurements for autonomous beating tissues and at the same time under external stretching of large deformations. On the other hand, our present method of measuring the IBI dynamics is very robust and can reveal various interesting dynamics resulting from the regulation from external stretching. Here by directly applying mechanical forces on the cardiac tissue, our results suggest a possible mechanism that the periodic stretching induces cyclic ion current and therefore affects the cardiac beating dynamics. The empirical coupling strength between external force and tissue can be deduced from our analytic results, providing additional insight on the entrained cardiac tissue beyond previous studies.

ACKNOWLEDGMENTS

This work has been supported by the Ministry of Science and Technology of ROC under Grants No. 107-2112-M-008-013-MY3, No. 108-2112-M-001-029-MY3, and NCTS of Taiwan.

APPENDIX A: DERIVATION OF EQ. (4)

By integrating Eq. (2), we obtain

$$\tan\frac{\psi(t)}{2} = \tilde{K} + \sqrt{1-\tilde{K}^2}\tan\left[\frac{\sqrt{1-\tilde{K}^2}}{2}(\omega-\Omega)(t-t_0)\right]. \tag{A1}$$

Here $\tilde{K} \equiv \frac{K}{\omega-\Omega}$, t_0 is the constant determined by the initial condition. By applying the initial condition that $\psi(0) = 0$, Eq. (A1) gives

$$\tan\left[\frac{\sqrt{1-\tilde{K}^2}}{2}(\omega-\Omega)t_0\right] = \frac{\tilde{K}}{\sqrt{1-\tilde{K}^2}} = \frac{K}{\sqrt{(\omega-\Omega)^2-K^2}} \equiv \beta. \tag{A2}$$

Next, we will show that the cardiac beating time can be obtained by finding the roots in a transcendental equation and therefore interbeat intervals. Using the identity $\tan(A-B) = (\tan A - \tan B)/(1+\tan A \tan B)$, Eq. (A1) can be rewritten as

$$\tan\frac{\psi(t)}{2} = \tilde{K} + \sqrt{1-\tilde{K}^2}\,\frac{\tan\left[\frac{\sqrt{1-\tilde{K}^2}}{2}(\omega-\Omega)t\right]-\beta}{1+\beta\tan\left[\frac{\sqrt{1-\tilde{K}^2}}{2}(\omega-\Omega)t\right]}. \tag{A3}$$

Define T_n as the time for the phase ϕ to be at of $2n\pi$, i.e., $\phi(T_n) = 2n\pi$, then $t = T_n$, $\psi(T_n) \equiv \psi_n = 2n\pi - \Omega T_n$, and hence Eq. (A3) gives

$$-\tan\frac{\Omega T_n}{2} = \tilde{K} + \sqrt{1-\tilde{K}^2}\,\frac{\tan\left[\frac{\sqrt{1-\tilde{K}^2}}{2}(\omega-\Omega)T_n\right]-\beta}{1+\beta\tan\left[\frac{\sqrt{1-\tilde{K}^2}}{2}(\omega-\Omega)T_n\right]}, \tag{A4}$$

which in turn gives Eq. (4).

APPENDIX B: EXPANSION OF B_n IN POWERS OF $\tilde{K}$: DERIVATION OF EQ. (5)

Analytical explicit formula of the IBI can be obtained by systematic expansion in powers of $\tilde{K}$ outlined as follows. For small $\tilde{K}$, one can expand the beating times T_n in powers of $\tilde{K}$ and write

$$T_n \simeq \alpha_n^{(0)} + \alpha_n^{(1)}\tilde{K} + \alpha_n^{(2)}\tilde{K}^2 + \cdots. \tag{B1}$$

Substitute into the transcendental equation (3), equating the coefficients of different powers of $\tilde{K}$ gives the equations for $\alpha_n^{(0)}, \alpha_n^{(1)}, \alpha_n^{(2)}, \ldots$. For instance,

$$\mathcal{O}(\tilde{K}^0): \ \tan\frac{\alpha_n^{(0)}}{2} + \tan\left[\left(\frac{\omega}{\Omega}-1\right)\frac{\alpha_n^{(0)}}{2}\right] = 0 \tag{B2}$$

$$\Rightarrow \alpha_n^{(0)} = \frac{2n\pi\Omega}{\omega}, \tag{B3}$$

$$\mathcal{O}(\tilde{K}^1): \ \frac{\alpha_n^{(1)}}{2}\mathrm{s}^2\frac{\alpha_n^{(0)}}{2} + 1 + \left(\frac{\alpha_n^{(1)}}{2}\left(\frac{\omega}{\Omega}-1\right)\right)\mathrm{s}^2\left[\left(\frac{\omega}{\Omega}-1\right)\frac{\alpha_n^{(0)}}{2}\right] = 0 \tag{B4}$$

$$\text{using (B3)} \Rightarrow \alpha_n^{(1)} = \frac{2\Omega}{\omega}\sin^2\frac{\alpha_n^{(0)}}{2} = \frac{2\Omega}{\omega}\sin^2\frac{n\pi\Omega}{\omega}. \tag{B5}$$

Since $B_n = T_{n+1} - T_n$, we have

$$B_n = \frac{2\pi}{\omega} + \frac{2\tilde{K}}{\omega}\sin\left(\frac{\Omega\pi}{\omega}\right)\sin\left[\frac{\Omega}{\omega}(2n+1)\pi\right] + \mathcal{O}(\tilde{K}^2).$$

[1] H. Tsuji, F. J. Venditti, E. S. Manders, J. C. Evans, M. G. Larson, C. L. Feldman, and D. Levy, Reduced heart rate variability and mortality risk in an elderly cohort. The Framingham Heart Study, Circulation **90**, 878 (1994).

[2] J. F. Thayer, S. S. Yamamoto, and J. F. Brosschot, The relationship of autonomic imbalance, heart rate variability and cardiovascular disease risk factors, Int. J. Cardiol. **141**, 122 (2010).

[3] C.-K. Peng, I. C. Henry, J. E. Mietus, J. M. Hausdorff, G. Khalsa, H. Benson, and A. L. Goldberger, Heart rate dynamics during three forms of meditation, Int. J. Cardiol. **95**, 19 (2004).

[4] A. Ben-Tal, S. S. Shamailov, and J. F. Paton, Central regulation of heart rate and the appearance of respiratory sinus arrhythmia: New insights from mathematical modeling, Math. Biosci. **255**, 71 (2014).

[5] G. A. R. del Paso, J. Godoy, and J. Vila, Self-regulation of respiratory sinus arrhythmia, Biol. Psychol. **35**, 17 (1993).

[6] P. C. Ivanov, Q. D. Ma, and R. P. Bartsch, Maternal-fetal heartbeat phase synchronization, Proc. Natl. Acad. Sci. USA **106**, 13641 (2009).

[7] P. Kohl, A. Kamkin, I. Kiseleva, and D. Noble, Mechanosensitive fibroblasts in the sino-atrial node region of rat heart: Interaction with cardiomyocytes and possible role, Exp. Physiol. **79**, 943 (1994).

[8] P. Camelliti, T. K. Borg, and P. Kohl, Structural and functional characterisation of cardiac fibroblasts, Cardiovasc. Res. **65**, 40 (2005).

[9] W. Y. Chiang, P. Y. Lai, and C. K. Chan, Frequency Enhancement in Coupled Noisy Excitable Elements, Phys. Rev. Lett. **106**, 254102 (2011).

[10] B. Frey, G. Heger, C. Mayer, B. Kiegler, H. Stöhr, and G. Steurer, Heart rate variability in isolated rabbit hearts, Pacing Clin. Electrophysiol. **19**, 1882 (1996).

[11] H. E. Stephenson, L. C. Reid, and J. W. Hinton, Some common denominators in 1200 cases of cardiac arrest, Ann. Surg. **137**, 731 (1953).

[12] T. Pellis and P. Kohl, Extracorporeal cardiac mechanical stimulation: Precordial thump and precordial percussion, Brit. Med. Bull. **93**, 161 (2009).

[13] M. J. Lab, Mechanoelectric feedback (transduction) in heart: Concepts and implications, Cardiovasc. Res. **32**, 3 (1996).

[14] K. Takahashi, Y. Kakimoto, K. Toda, and K. Naruse, Mechanobiology in cardiac physiology and diseases, J. Cell. Mol. Med. **17**, 225 (2013).

[15] G. Hasenfuss, L. A. Mulieri, E. M. Blanchard, C. Holubarsch, B. J. Leavitt, F. Ittleman, and N. R. Alpert, Energetics of isometric force development in control and volume-overload human myocardium. Comparison with animal species, Circ Res. **68**, 836 (1991).

[16] J. van der Velden, L. J Klein, M. van der Bijl, M. A. J. M. Huybregts, W. Stooker, J. Witkop, L. Eijsman, C. A. Visser, F. C. Visser, and G. J. M. Stienen, Force production in mechanically isolated cardiac myocytes from human ventricular muscle tissue, Cardiovasc. Res. **38**, 414 (1998).

[17] S. Barni, F. Bernini, C. Fenoglio, and C. Reggiani, Adaptations of the frog myocardium to conditions of natural hibernation: Morphofunctional changes, Boll. Zool. **61**, 317 (1994).

[18] D. Sasaki, K. Matsuura, H. Seta, Y. Haraguchi, T. Okano, and T. Shimizu, Contractile force measurement of human induced pluripotent stem cell-derived cardiac cell sheet-tissue, PLoS ONE **13**, e0198026 (2018).

[19] F. A. Bainbridge, The influence of venous filling upon the rate of the heart, J. Physiol. **50**, 65 (1915).

[20] G. Lange, H. Lu, A. Chang, and C. Brooks, Effect of stretch on the isolated cat sinoatrial node, Am. J. Physiol.-Legacy Content **211**, 1192 (1966).

[21] D. Kelly, L. Mackenzie, P. Hunter, B. Smaill, and D. Saint, Gene expression of stretch-activated channels and mechanoelectric feedback in the heart, Clin. Exp. Pharmacol. Physiol. **33**, 642 (2006).

[22] T. A. Quinn and P. Kohl, Mechano-sensitivity of cardiac pacemaker function: Pathophysiological relevance, experimental implications, and conceptual integration with other mechanisms of rhythmicity, Prog. Biophys. Mol. Biol. **110**, 257 (2012).

[23] K. A. Deck, Dehnungseffekte am spontanschlagenden, isolierten Sinusknoten, Pfluegers Archv. **280**, 120 (1964).

[24] P. J. Cooper, M. Lei, L.-X. Cheng, and P. Kohl, Selected contribution: Axial stretch increases spontaneous pacemaker activity in rabbit isolated sinoatrial node cells, J. Appl. Physiol. **89**, 2099 (2000).

[25] M. Guevara, L. Glass, and A. Shrier, Phase locking, period-doubling bifurcations, and irregular dynamics in periodically stimulated cardiac cells, Science **214**, 1350 (1981).

[26] S. H. Strogatz, *Nonlinear Dynamics and Chaos: With Applications to Physics, Biology, Chemistry, and Engineering*, 2nd ed. (Westview, Boulder, 2015).

[27] W. Zeng, L. Glass, and A. Shrier, Evolution of rhythms during periodic stimulation of embryonic heart cell aggregates, Circ. Res. **69**, 1022 (1991).

[28] M. R. Guevara and A. Shrier, Rhythms produced by high-amplitude periodic stimulation of spontaneously beating aggregates of embryonic chick ventricular myocytes, Ann. N.Y. Acad. Sci. **591**, 11 (1990).

[29] Y. Yaniv, E. G. Lakatta, and V. A. Maltsev, From two competing oscillators to one coupled-clock pacemaker cell system, Front. Physiol. **6**, 28 (2015).